Performance evaluation of Wavewatch III in the Mediterranean Sea

Lorenzo Mentaschi [a,c,*], Giovanni Besio [a], Federico Cassola [b,c,d], Andrea Mazzino [a,c,d]

[a] DICCA, Dipartimento di Ingegneria Civile, Chimica e Ambientale, Via Montallegro 1, 16145 Genova, Università degli Studi di Genova, Italy
[b] DIFI, Dipartimento di Fisica, Via Dodecaneso 33, 16146, Genova, Università degli Studi di Genova, Italy
[c] INFN, Istituto Nazionale di Fisica Nucleare, Sezione di Genova, Via Dodecaneso 33, Genova, 16146, Italy
[d] Consorzio CINFAI, Sezione di Genova, Via Montallegro 1, Genova, 16145, Italy

ARTICLE INFO

ABSTRACT

For this study, we analyzed the performance of the wave model Wavewatch III® forced by a limited area atmospheric model in the Mediterranean Sea. The simulation results have been compared to buoy measurements through single point statistical indicators such as normalized bias and symmetrically normalized root mean square error. A performance evaluation of the growth-dissipation source terms and their reference parameterizations was carried out on seventeen case studies corresponding to storms in the Northern Tyrrhenian Sea and off the Mediterranean Spanish coast. The source terms introduced by Ardhuin et al. (2010) proved to be the best overall choice, although they led to an overestimation in the significant wave height under calm conditions and to an underestimation under severe conditions. A sensitivity analysis in the parameter space was performed within the neighborhood of the reference parameterization of Ardhuin et al. (2010), and a calibration was carried out to reduce the overall positive bias in the significant wave height. Furthermore, to investigate the effect from the wind forcing resolution, wind data with different resolutions was used in a sensitivity analysis. Because mesoscale features are relevant to the overall Mediterranean wave dynamics, we carried out a further investigation into the impact of the resolution on a different set of ten case studies characterized by strong mesoscale patterns. A comparison of the simulations with the measurements using single point statistical indicators shows that the high resolution results are affected by the so-called double penalty effect, although in some cases, they apparently provide a better qualitative description of the event. Finally, a hindcast covering 32 years (from 1979 to 2010) was developed using a reference parameterization from Ardhuin et al. (2010) and its calibrated variant. An analysis of the performance of the calibrated parameterization on the hindcast dataset reveals that it performs better than the reference parameterization over a wide range of wave heights, in seas that range from calm to moderate, whereas it increases the tendency to underestimate the significant wave height under severe conditions.

© 2015 Elsevier Ltd. All rights reserved.

1. Introduction

Atmospheric and wave modeling in the Mediterranean Sea encounter specific issues compared to open oceans, due to the complexity of the surrounding orography, which involves strongly local meteorological characteristics, and due to the complex bathymetry and limited fetch extension. Under these conditions, aspects that usually have negligible or relatively reduced effects in an open ocean, such as mesoscale meteorological features or wave interactions with the bathymetry and with small obstacles, are relevant to the overall atmosphere-ocean dynamics in the Mediterranean.

In this context, continuous efforts to improve different aspects of wave simulations in third-generation wave models (i.e., wave models with a punctual, though approximate, representation of non linear wave–wave interactions Komen et al., 1994) in enclosed basins or marginal seas, such as the Mediterranean produce a better representation of local wave dynamics. Particularly significant progress in this direction was obtained by Ardhuin et al. (2010) due to the introduction of new source terms for wave growth and dissipation. Originally, these source terms were developed to reproduce in a Wavewatch III® model (hereinafter WWIII) the growth and dissipation description already present in the operational WAM model at ECMWF (Bidlot et al., 2007), based on a theory of wave growth by Miles (1957) and subsequently improved by Janssen (1982). The description of the wave dissipation is based on a semiempirical representation of the whitecapping phenomena and on saturation spectrum approaches (Ardhuin et al., 2008, 2010; Hasselmann, 1974; Komen et al., 1984; Phillips, 1985). An innovative contribution of Ardhuin et al. (2010) consists of

* Corresponding author at: DICCA, Dipartimento di Ingegneria Civile, Chimica e Ambientale, Via Montallegro 1, 16145 Genova, Università degli Studi di Genova, Italy. Tel.: +390103536576.
E-mail address: lorenzo.mentaschi@unige.it, lorenzo.mentaschi@yahoo.it (L. Mentaschi).
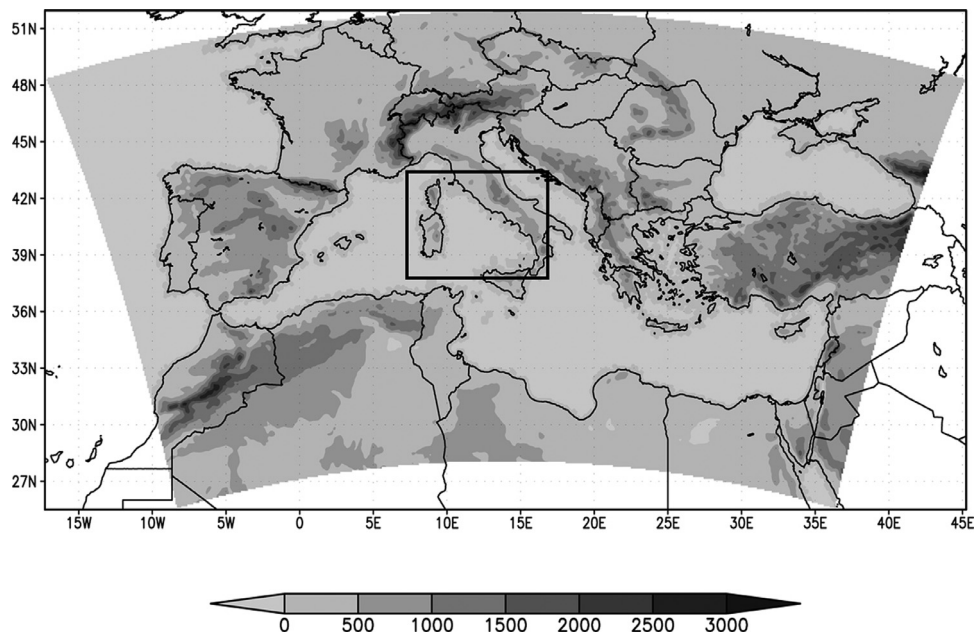
Fig. 1. Integration domain of WRF. The box on the Tyrrhenian Basin represents the A3 domain.

a new term to describe long swell dissipation as a function of the drag velocity. Comparisons between the model results and observations obtained from satellites and buoys indicates a significant improvement in global scale simulations (Ardhuin et al., 2008, 2010).

Extending the work of Mentaschi et al. (2013a), we evaluated the performance of the numerical model WWIII in the Mediterranean Sea, forced by the atmospheric model Weather and Research Forecasting (hereinafter WRF). The simulations were carried out on seventeen case studies corresponding to storms in the northern Tyrrhenian Sea and off the Mediterranean Spanish coast. The reliability of the results was assessed to compare the numerical results with buoy data provided by RON (Rete Ondametrica Nazionale) and by the Spanish network of deep water buoys REDEXT (Red Exterior) of significant wave height H_s, mean period $T_m = T_{-1,0}$ and mean direction θ_m. The comparison between the simulated and observed data was performed through single point statistical indicators such as the normalized bias (*NBI*), correlation coefficient (ρ) and symmetrically normalized root mean square error (*HH,* Hanna and Heinold, 1985; Mentaschi et al., 2013b). This analysis was carried out using wind data downscaled to different resolutions of 10 km and 20 km and was performed using the reference parameterization from Ardhuin et al. (2010). A further calibration of this parameterization led to a slight reduction in the wave growth reference parameterization. An investigation into the role of resolution in the Mediterranean context was performed on another set of case studies, which corresponded to storms on the Tyrrhenian Sea that were characterized by distinct mesoscale features. Event selection was undertaken to isolate situations that were specific to the Mediterranean Sea that are difficult to identify using coarse resolution simulations.

On the basis of this analysis, a 32-year hindcast dataset was developed covering the years from 1979 and 2010. This reanalysis was carried out using both the reference parameterization from Ardhuin et al. (2010) and the calibrated parameters set found in the analysis of the seventeen case studies. Hindcast was validated using buoy data provided by RON, REDEXT and the Poseidon Greek buoys network.

In the following section, WRF and WWIII models and their settings are illustrated. Section 3 illustrates the methodology employed for model performance evaluation, whereas in section 4, a sensitivity analysis on the space parameters and model calibration are reported. Some conclusions are drawn in Section 5 about the role of the

wind forcing resolution. An analysis of mesoscale event simulations is described in Section 6. Section 7 illustrates the 32-year hindcast validation, together with some considerations about the bathymetry resolution at different buoy locations.

2. Overview of models and settings

The numerical modeling chain employed in this study consists of an atmospheric model for downscaling wind and atmospheric fields and a third-generation model for wave generation and propagation in the Mediterranean Sea.

2.1. Atmospheric model

The wind forcing employed in the simulations was provided by 10-m wind fields that were obtained from the non-hydrostatic mesoscale model Weather Research and Forecast (WRF-ARW) version 3.3.1 (Skamarock et al., 2008). The application of a high-resolution mesoscale model allows for better representation of small-scale forcings triggered by topographic features and for incorporation of the dynamics and physics affecting the smaller scales, thereby producing a physically consistent downscaling of larger scale simulations.

In this study, the following computational domains were employed (see Fig. 1):

- a Lambert conformal grid with a 10 km resolution over the whole Mediterranean Sea, Northern Africa and Southern Europe. This grid is hereinafter referred to as A10;
- a grid similar to the one described above, but with a resolution of 20 km. This grid is hereinafter referred to as A20;
- a Lambert conformal grid with a resolution of approximately 3.3 km covering the Tyrrhenian Basin. This domain, hereinafter referred to as A3, was two-way nested in the A10 grid.

Topography, land use and land-water masked datasets were interpolated from the 2′-resolution USGS datasets. Initial and boundary conditions for the atmospheric simulations with the WRF model were provided from the CFSR (Climate Forecast System Reanalysis) database (Saha et al., 2010). Use of CFSR reanalysis data for wave modeling usually guarantees good performance, although it sometimes leads to an underestimation of the most extreme events (e.g.
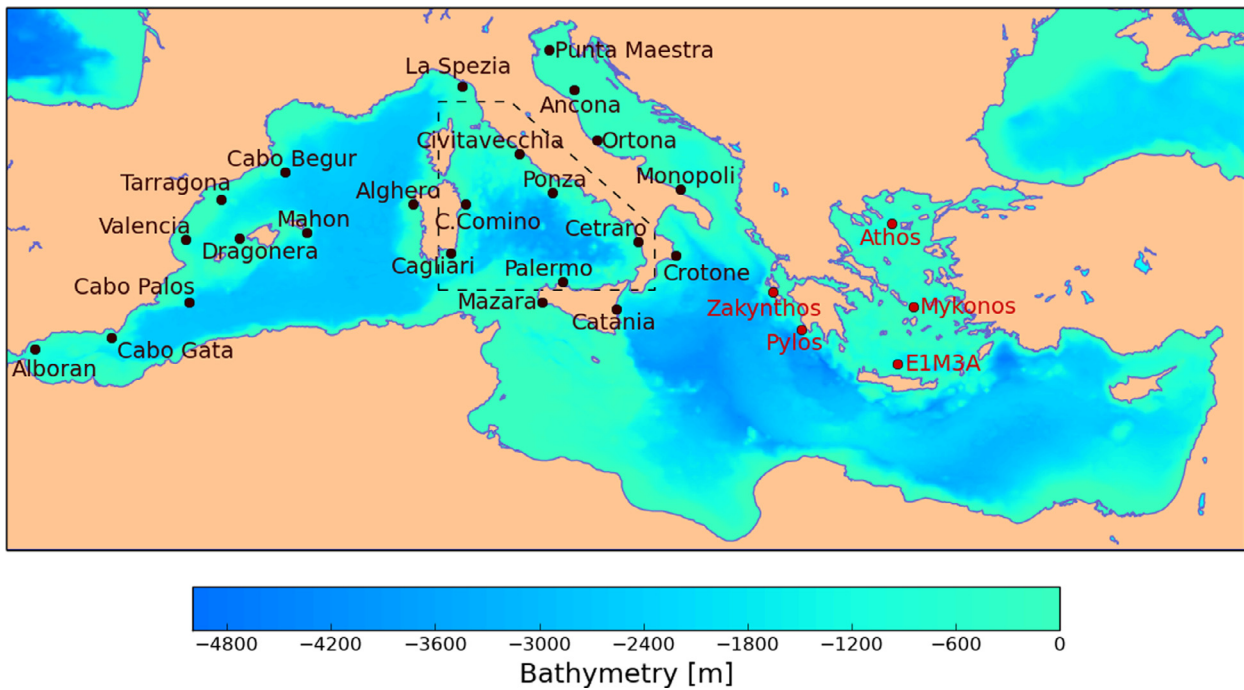
Fig. 2. Integration domain of WWIII. The dashed box on the Tyrrhenian Basin represents the R2 domain. The buoys marked with black dots were used for performance evaluation. For hindcast validation, the buoys marked with red dots were also used. (For interpretation of the references to color in this figure legend, the reader is referred to the web version of this article.)

Cox et al., 2011; Splinder et al., 2011; Chawla et al., 2013; Carvalho et al., 2012).

For each of the examined case studies, a 24-h-long reforecast running mode with a cold start was adopted for the WRF simulations; the outputs were saved every hour and the analysis was updated every 24 h, whereas the boundary conditions were imposed every 3 h. This type of approach leads to unavoidable discontinuities in the wind fields every 24 h. However, this is a minor drawback as the influence of such discontinuity on the wave field is reasonably small due to the delayed response of wave growth and development to wind forcing. On the other hand, creating a continuous WRF simulation (approximately 10 days long in each case study) would certainly trigger significant errors in the wind output because longer-term forecasts progressively drift away from reality, compensating the advantage of eliminating discontinuities.

A full set of well-known and widely used physical parameterization schemes were adopted, following Bove et al. (2014) and Cassola et al. (2015). For long-wave radiation, a Rapid Radiation Transfer Model (RRTM) was selected (Mlawer et al., 1997), whereas for short-wave solar radiation, a Goddard scheme was adopted (Chou and Suarez, 1994). The Kain-Fritsch parameterization (Kain, 2004) was used for the cumulus in coarser resolution simulations (20-km and 10-km resolution domains), whereas in the finest resolution domain (3.3 km), the convection could be explicitly resolved. The Mellor–Yamada–Janjic (MYJ PBL) scheme (Janjic, 2002) was used for the boundary layer, and the Thompson scheme (Thompson et al., 2008) was used for the microphysics. Finally, the Eta similarity surface layer scheme (Janjic, 2002) and the Noah land surface model (Chen and Dudhia, 2001) were adopted.

2.2. Wave model

In this study, we relied on the third-generation Wavewatch III® model, version 3.14 (Tolman, 2009) for wave modeling. The following computational domains were employed:

- a regular grid covering the whole Mediterranean Sea with a resolution of $0.1273° \times 0.09°$, corresponding to approximately 10 km at a latitude of 45°N. This grid is hereinafter referred to as R10;
- a grid similar to R10 but with a resolution of $0.2546° \times 0.18°$, corresponding to approximately 20 km at a latitude of 45°N. This domain is hereinafter referred to as R20;
- a regular grid covering the Tyrrhenian Sea with a resolution of $0.02546° \times 0.018°$, corresponding to approximately 2 km at a latitude of 45°N, hereinafter referred to as R2. This grid was nested into the R10 grid.

The WWIII integration domains are represented in Fig. 2 together with the buoys used for the performance evaluation. The spectral domain consists of 25 frequencies separated by a factor of 1.1 integrated on 24 different directions. The maximum period for consideration was 15 s and the minimum period was approximately 1.4 s.

The wave model was forced with the wind fields modeled by the atmospheric model with an hourly time step. The output was recorded hourly at all points on the computational grid to determine the integrated quantities (H_s, T_m, θ_m), whereas the wave spectra were stored at the coordinates corresponding to the locations of the wave buoys. A comparison between the numerical results and the observations was performed employing integrated parameters, such as the significant wave height H_s, the mean wave period T_m and the mean propagation direction θ_m. Model performance depends on the sea conditions, therefore, the error measurements were evaluated in different groups of buoys that were selected for each case study, depending on the local sea conditions (stormy or not stormy).

2.2.1. Source terms and parameterizations

WWIII is a third-generation model (Tolman, 2009) based on the integration of wave spectral action balance equation, which states that the evolution of the wave field is controlled by a sum of source terms consisting of the transfer of energy from the wind field to the waves through a wind-wave interaction term (S_{in}), the dissipation due to wave breaking (S_{ds}) and the nonlinear interactions between waves

Table 1
Ardhuin et al. (2010) parameterization ACC350: parameter values, minimum and maximum values employed in the sensitivity analysis. Values of parameters not showed in this table assume a zero value.

Parameter	WWIII variable	ACC350 Val.	Min.	Max.
α_0	alpha0	0.0095	0.009	0.01
β_{max}	betamax	1.75	1.5	2
p_{in}	sinthp	1.7	1.5	1.9
z_α	zalp	0.004	0.003	0.005
s_u	tauwshelter	-1	-1.5	-0.5
s_1	swellf	0.7	0.5	0.9
s_2	swellf2	-0.018	-0.024	-0.012
s_3	swellf3	-0.015	-0.02	-0.01
z_r	z0rat	0.04	0.03	0.05
c_{ds}	sdsc1	-4	-5	-3
p	wnmeanp	0.5	-0.5	1.5
δ_1	sdsdelta1	0.4	0.3	0.5
δ_2	sdsdelta2	0.6	0.5	0.7
C_{ds}^{sat}	sdsc2	-2.2×10^{-5}	-2.6×10^{-5}	-1.8×10^{-5}
Δ_θ	sdsdth	70	40	100
b_r	sdsbr	1.2×10^{-3}	1×10^{-3}	1.4×10^{-3}
b_{r2}	sdsbr2	1	0.5	1.5
B_0	sdsc4	1	0.9	1.1
p^{sat}	sdsp	2	1.8	2.2
$c_{ds, 6}$	sdsc6	0.25	0.21	0.29
s_0	swellfpar	3	–	–
s_{m0}	sdsbm0	1	–	–
z_u	zwnd	10	–	–
Re_c	swellf4	100, 000	–	–

(S_{nl}). What distinguishes third-generation models from older ones is a punctual, although approximate, representation of wave-wave nonlinear interactions through the Discrete Interaction Approximation (DIA, Hasselmann and Hasselmann, 1985). Because nonlinear wave–wave interactions are responsible for the energy cascade from high-frequency to low-frequency modes, the adoption of DIA approximation represents an important improvement in the numerical simulation of wave dynamics.

In this study, we employed growth-dissipation source terms developed by Ardhuin et al. (2010), while using the set of parameters named ACC350[1] in the WWIII user guide (Tolman, 2009). This set introduced a dissipation term for the swell as a function of the wind drag velocity, which improves the distinction between wave growth and dissipation forced by the wind.

The behavior of the parameterization was analyzed through a sensitivity analysis performed in the neighborhood of the default values of the reference parameterization, varying the value of each parameter within a range centered on its reference value. The maximum and minimum values used for each parameter in the analysis are listed in Table 1 together with the reference value for the ACC350 parameterization.

For the sake of completeness, the parameterization of Bidlot et al. (2007), is from now on referred to as BJA, and the source terms of Tolman and Chalikov (1996) in their reference parameterization are from now on referred to as TC, were also taken into account in the comparison between the numerical results and the buoy data. For details about TC and BJA parameterizations the reader is referred to Tolman (2009). In total, 44 different parameterizations have been tested for all of the seventeen case studies.

3. Performance evaluation methodology

The performance evaluation of the model system was carried out by comparing the simulated variables with buoy measurements provided by the Rete Ondametrica Nazionale (RON, Italy) and by the Red

Externa (REDEXT, Spain) through single point statistical indicators. The positions of the buoys are illustrated in Fig. 2 (only buoys marked with black dots). By saying "single point indicators", we mean that the variables have been compared at each time step for given points in the domain (in this study the buoy positions).

To evaluate the scatter component of the scalar quantities error, we decided not to rely on the traditional error indicators (Scatter Index SI and Normalized Root Mean Square Error $NRMSE$), exploiting instead the symmetrically normalized root mean square error (HH) (Hanna and Heinold, 1985; Mentaschi et al., 2013b). This has been the choice since Mentaschi et al. (2013b) showed that in some cases simulations affected by negative bias tend to present smaller values of $RMSE$ and tend to be identified as performing better than unbiased simulations. The error indicator introduced by Hanna and Heinold (1985) overcomes this drawback and allows it to have more complete synthetic information about the performance of the model.

Therefore, the statistical indicators employed in this study for scalar integrated quantities (e.g., significant wave height and mean period) are as follows:

- the Normalized Bias $NBI = \Sigma(S_i - O_i)/\Sigma O_i$, where S_i and O_i are simulations and observations, respectively. This is an indicator of the average component of the error, and a value closer to zero indicates a better simulation;
- the Correlation Coefficient $\rho = \sum (S_i - \bar{S})(O_i - \bar{O})/\sigma_S\sigma_O$ where σ_S and σ_O are the standard deviation of simulations and observations, respectively. This is an indicator of the scatter component of the error, and a value closer to one indicates a simulation that is less affected by random error;
- the symmetrically normalized root mean square error HH introduced by Hanna and Heinold (1985) $HH = \sqrt{\sum (S_i - O_i)^2 / \sum S_i O_i}$. This indicator combines information about the average and scatter components of the error, and, as already mentioned, it is not biased towards simulations that underestimate the average (see Mentaschi et al., 2013b, for a discussion on RMS and Scatter Index indicators).

For circular quantities, such as the mean direction, the normalized bias NBI_θ and the normalized root mean square error $NRMSE_\theta$, have been normalized employing a 2π radiants angle:

- $NBI_\theta = \dfrac{\sum \mathbf{mod}_{-\pi,\pi} (\theta_{si} - \theta_{oi})}{2\pi N}$;

- $NRMSE_\theta = \dfrac{\sqrt{\sum [\mathbf{mod}_{-\pi,\pi} (\theta_{si} - \theta_{oi})]^2/N}}{2\pi}$,

where the modulo operator $\mathbf{mod}_{-\pi, \pi}$ indicates that if $(\theta_{si} - \theta_{oi}) > \pi$ a 2π angle is subtracted from the difference, if $(\theta_{si} - \theta_{oi}) < -\pi$ a 2π angle is added to the difference. Finally, to provide a graphical representation of the results, Taylor diagrams (Taylor, 2001; Tolman et al., 2013) and diagrams representing the correlation coefficient versus the normalized bias were produced.

4. Performance evaluation

4.1. Case studies

Seventeen case studies were selected for the WWIII performance evaluation to represent the typical storm conditions in the Mediterranean Sea. These events are the same as those already considered in Mentaschi et al. (2013a, 2013b) and were chosen using a peak over threshold criterion, namely, a significant wave height greater than 4 m at two buoys or more. Table 2 reports the time scale of each case study, the maximum measured significant wave height and mean period over the whole buoy data set.

Among the considered events, some exhibited distinct synoptic scale patterns (i.e., on a length scale of 1000 km or more),

---

[1] The acronym ACC350 refers to the authors F. Ardhuin, F. Collard and B. Chapron, who developed a term describing long swell decay, based on a study of Synthetic Aperture Radar observations (Ardhuin et al., 2008, 2009).

Table 2
Case studies considered for a sensitivity analysis in the parameter space. Maximum significant wave height and maximum mean period are referred to in the available buoy records.

Case study	Start date	End date	Max H_s [m]	Max T_m [s]
February 1990	24/02/1990	05/03/1990	7.10	10.5
December 1999	23/12/1999	29/12/1999	9.88	11.5
November 2000	01/11/2000	10/11/2000	5.77	9.7
February 2004	19/02/2004	27/02/2004	6.00	9.2
April 2004	24/04/2004	09/05/2004	4.90	9.4
February 2005	26/02/2005	03/03/2005	4.80	8.6
November 2005	24/11/2005	01/12/2005	4.60	8.0
December 2006	04/12/2006	12/12/2006	5.20	9.5
November 2007	30/11/2007	07/12/2007	6.06	8.7
March 2008	18/03/2008	24/03/2008	5.60	9.9
October 2008	26/10/2008	03/11/2008	5.00	7.2
November 2009	26/11/2009	05/12/2009	4.20	7.4
January 2010	26/01/2010	05/02/2010	4.70	7.2
February 2010	15/02/2010	23/02/2010	6.59	11.8
March 2010	24/03/2010	04/04/2010	4.70	10.0
May 2010	01/05/2010	07/05/2010	5.60	8.4
November 2011	02/11/2011	11/11/2011	5.23	9.8

whereas others also present distinct mesoscale features (i.e., at a length scale of 100 km). In particular, we consider purely "synoptic" events to be those dominated by very large-scale disturbances, typically embedded in a strong zonal flow across Central Europe and the Mediterranean Basin. In contrast, "mesoscale" events are associated with smaller-scale patterns, essentially secondary Mediterranean cyclones (more details about Mediterranean cyclogenesis are given in Section 6).

More specifically, eight out of the seventeen case studies were mainly "synoptic" (namely, February 1990, December 1999, November 2000, February 2005, November 2005, November 2007, November 2009 and January 2010); eight exhibit both synoptic and mesoscale characteristics (February 2004, April 2004, December 2006, March 2008, October 2008, February 2010, March 2010 and November 2011); and one (May 2010) is a clear mesoscale event, with a deep small-scale cyclone over the Western Mediterranean moving towards Southern France and Northern Italy.

Most of these events are associated with strong south-southwesterly winds at an early stage, then veering to westerly-northwesterly as the storm moves eastward, thereby affecting first the Ligurian coast (which is well exposed to Ostro and Libeccio winds), then affecting the Tyrrhenian Sea and the Western Mediterranean (Ponente and Mistral). In particular, the December 1999 event produced the strongest wave conditions ever recorded at several Italian buoys. Other cases were characterized by intense easterly-northeasterly winds (Levante and Gregale) affecting the Western Mediterranean and the Iberian coast, where buoy data were available (namely, February 1990, February 2004, April 2004, February 2005, January 2010).

4.2. Sensitivity analysis in parameter space

In this section, we examine the results of the sensitivity analysis in parameters space. The set of parameterizations employed in this analysis is described in Section 2.2.1 and includes the reference parameterizations ACC350, BJA and TC and 40 additional parameterizations obtained by varying each parameter of ACC350.

This analysis was repeated by employing wind data elaborated with A WRF set up using grids A10 and A20. The two resulting datasets are hereinafter referred to as V-10-10 and V-20-10, respectively (in the abbreviation V-X-Y, V stands for "validation", X is the resolution of the wind field, Y is the resolution of the wave field). In Table 3 the values of NBI and HH evaluated for the two datasets (which include

42,100 records each) are reported for significant wave height and mean period for all of the considered parameterizations.

The performances analysis shows that TC is generally affected by a relevant negative bias for both the significant wave height H_s and the mean period T_m. Taking into account the whole set of case studies, the bias for TC in the V-10-10 run was found to be approximately −12.3% for the significant wave height and approximately −12.7% for the mean period. These figures may result from the default settings of the source terms of Tolman and Chalikov (1996) having been developed and optimized for oceanic wave conditions, which differ from those existing in the Mediterranean Sea. A possible explanation is that in open ocean (where the swell component is prevalent, e.g. Chen et al., 2002; Semedo et al., 2011), an underestimation of the wind sea (Pierson and Moskowitz, 1964) may be whole compensated by the overestimation of the swell due to a less advanced description of the long swell dissipation (Tolman and Chalikov, 1996). Conversely, the wave dynamics in the Mediterranean Sea under storm conditions are dominated by local wave generation, and swell decay attains a secondary role (in open ocean swell the e-folding scale exceeds 20,000 km, shrinking to 2800 km for the steepest observed swells, Ardhuin et al., 2009). Another possible explanation for the strong negative bias is the large fraction of fetch-limited sea winds that exist in the Mediterranean Sea; the wave generation term of Tolman and Chalikov (1996) is optimized for the long fetch that exists in the ocean and may perform worse when modeling less developed wind sea conditions. However, it is worth noting that the simulations obtained with the source terms by Tolman and Chalikov (1996) present correlation coefficients that are better than simulations obtained with other source terms, especially for the mean period.

The BJA parameterization of Ardhuin et al. (2010) source terms partially reduces the overall underestimation of the significant wave height and the mean period, because the bias estimated for the whole V-10-10 dataset is approximately −5% for the significant wave height and approximately −3.8% for the mean period. Finally, ACC350 parameterization leads to a further reduction in the underestimation of local generation, due to its new term of swell dissipation that allows an overall better balance between the wind sea and swell. The overall bias in the significant wave height for the case studies is indeed slightly positive, with a value of 1.6%, whereas for the mean period, it is −3.4%. In this respect, we found that ACC350 parameterization gives a more accurate description of wave dynamics in the Mediterranean Sea.

The results of the analysis for the V-10-10 dataset are shown in Fig. 3, where the bias of the significant wave height and the mean period are plotted against the correlation coefficient and in Fig. 4, where Taylor diagrams are presented. From these graphs, it is possible to observe that all of the parameterizations present similar correlation coefficient values, whereas the bias range is rather large. Mentaschi et al. (2013b) showed that if a correlation coefficient presents a constant value in the neighborhood of a null bias, a simulated time series S_{Bi} with normalize bias $NBI = B$ can be expressed as

$$S_{Bi} = \alpha_B S_{0i}, \qquad (1)$$

where S_{0i} is an unbiased time series independent from the series S_{Bi} and the scaling factor α_B is given by $\alpha_B = (1 + B)$. Therefore, the results obtained for different parameterizations roughly follow the relationship (1) and are roughly proportionate to each other.

The fact that for all of the employed parameterizations, the correlation coefficients between the simulated and observed quantities present similar values may be due to the characteristics of the examined case studies, which represent typical Mediterranean storms: in fact, the selected cases are generated by intense short fetch events, and because the shape of the predominant locally generated portion of the wave spectrum is strongly dependent on the patterns followed by wind forcing, the scatter component of the error may be

Table 3
Indicators of *NBI* and *HH* for significant wave height and a mean period for all of the tested parameterizations, which were evaluated from the whole dataset of V-10-10 and V-20-10.

Parameterization	V-10-10				V-20-10			
	H_s		T_m		H_s		T_m	
	NBI	*HH*	*NBI*	*HH*	*NBI*	*HH*	*NBI*	*HH*
ACC350	0.016	0.288	−0.034	0.272	−0.003	0.302	−0.038	0.276
DICCA	0.003	0.286	−0.037	0.273	−0.020	0.301	−0.044	0.276
BJA	−0.050	0.292	−0.038	0.277	−0.068	0.310	−0.042	0.281
TC	−0.123	0.303	−0.127	0.301	−0.134	0.322	−0.131	0.305
alpha0 = 0.009	0.015	0.288	−0.034	0.271	−0.004	0.302	−0.038	0.276
alpha0 = 0.01	0.017	0.288	−0.033	0.272	−0.002	0.303	−0.038	0.276
betamax = 1.5	−0.049	0.287	−0.056	0.275	−0.067	0.305	−0.060	0.279
betamax = 2	0.071	0.301	−0.016	0.271	0.050	0.312	−0.020	0.275
sdsbr2 = 0.5	0.016	0.288	−0.034	0.272	−0.003	0.302	−0.038	0.276
sdsbr2 = 1.5	0.016	0.288	−0.034	0.272	−0.003	0.302	−0.038	0.276
sdsbr = 1.4E-3	0.102	0.304	−0.013	0.269	0.083	0.314	−0.017	0.273
sdsbr = 1E-3	−0.086	0.301	−0.060	0.277	−0.106	0.321	−0.065	0.282
sdsc1 = −3	0.016	0.288	−0.034	0.272	−0.003	0.302	−0.038	0.276
sdsc1 = −5	0.016	0.288	−0.034	0.272	−0.003	0.302	−0.038	0.276
sdsc2 = −1.8E-5	0.053	0.293	−0.025	0.270	0.034	0.306	−0.029	0.275
sdsc2 = −2.6E-5	−0.014	0.287	−0.041	0.273	−0.033	0.303	−0.046	0.277
sdsc4 = 0.9	−0.004	0.288	−0.039	0.272	−0.023	0.304	−0.043	0.277
sdsc4 = 1.1	0.036	0.289	−0.029	0.271	0.017	0.302	−0.033	0.275
sdsc6 = 0.21	0.018	0.288	−0.035	0.272	−0.001	0.302	−0.039	0.276
sdsc6 = 0.29	0.014	0.288	−0.033	0.271	−0.005	0.302	−0.037	0.276
sdsdelta1 = 0.3	0.016	0.288	−0.034	0.272	−0.003	0.302	−0.038	0.276
sdsdelta1 = 0.5	0.016	0.288	−0.034	0.272	−0.003	0.302	−0.038	0.276
sdsdelta2 = 0.5	0.016	0.288	−0.034	0.272	−0.003	0.302	−0.038	0.276
sdsdelta2 = 0.7	0.016	0.288	−0.034	0.272	−0.003	0.302	−0.038	0.276
sdsdth = 100	0.000	0.288	−0.030	0.271	−0.019	0.304	−0.035	0.276
sdsdth = 40	0.079	0.297	−0.023	0.269	0.060	0.308	−0.027	0.273
sdsp = 1.8	0.047	0.295	−0.027	0.271	0.028	0.307	−0.031	0.275
sdsp = 2.2	−0.011	0.285	−0.040	0.272	−0.030	0.301	−0.044	0.276
sinthp = 1.5	0.020	0.289	−0.033	0.271	0.001	0.303	−0.037	0.276
sinthp = 1.9	0.013	0.288	−0.035	0.272	−0.007	0.302	−0.039	0.276
swellf2 = −0.012	0.013	0.289	−0.036	0.272	−0.007	0.303	−0.040	0.276
swellf2 = −0.024	0.020	0.288	−0.032	0.271	0.001	0.302	−0.036	0.275
swellf3 = −0.01	0.023	0.288	−0.031	0.271	0.003	0.301	−0.035	0.275
swellf3 = −0.02	0.010	0.289	−0.036	0.272	−0.009	0.303	−0.041	0.276
swellf = 0.5	0.024	0.288	−0.031	0.271	0.004	0.301	−0.036	0.275
swellf = 0.9	0.010	0.289	−0.036	0.272	−0.009	0.304	−0.040	0.276
tauwshelter = −0.5	0.043	0.299	−0.027	0.272	0.022	0.311	−0.032	0.276
tauwshelter = −1.5	−0.012	0.282	−0.042	0.271	−0.030	0.298	−0.046	0.276
wnmeanp = −0.5	0.016	0.288	−0.034	0.272	−0.003	0.302	−0.038	0.276
wnmeanp = 1.5	0.016	0.288	−0.034	0.271	−0.003	0.302	−0.038	0.276
z0rat = 0.03	0.017	0.288	−0.033	0.271	−0.002	0.302	−0.038	0.276
z0rat = 0.05	0.016	0.288	−0.034	0.272	−0.004	0.302	−0.038	0.276
zalp = 0.003	−0.012	0.288	−0.045	0.273	−0.032	0.304	−0.050	0.278
zalp = 0.005	0.046	0.291	−0.021	0.270	0.027	0.303	−0.026	0.274

largely due to the approximate representation of wind forcing. Conversely, the bias of the significant wave height and mean period is strongly conditioned by the ability of the source terms to represent the wave growth corresponding to the average atmospheric input. This hypothesis is enforced if the analysis is carried out distinguishing between storm and non-storm conditions. Storm conditions have been identified at each buoy for each considered event using a peak over threshold criterion (a significant wave height greater than 2.5 m for at least 6 h). Comparing Figs. 3 and 5, we can see that the range of the correlation coefficient ρ between the simulated and observed variables under storm conditions is smaller than that found for the buoys under non-storm conditions; therefore, the effects of the different parameterizations on the correlation coefficients is smaller when local generation is stronger.

4.3. Model calibration

The results discussed in Section 4.2 show that variations of the parameters of growth-dissipation source terms have a small impact on the scatter component of the error for both the significant wave height and mean period under severe sea conditions. For this reason,

we decided to calibrate the model on the basis of the significant wave height bias. Because the reference parameterization in the V-10-10 dataset presents a slight positive bias in the significant wave height (see Figs. 3 and 4 and Table 3), we performed a calibration of the model by adjusting the value of the parameter β_{max}, which is a non-dimensional quantity proportionate to the wind-wave energy transfer (see Ardhuin et al., 2010; Tolman et al., 2013, for further detail). This parameter was adjusted to reduce a systematic slight overestimation in the significant wave height. The tuning process led to a reduction in β_{max} to a value of 1.68 from its original value of 1.75. The calibrated parameter set is hereinafter labeled as DICCA, to distinguish it from the reference parameterization ACC350.

5. The role of wind field resolution

These considerations confirm that the resolution of wind forcing is a main source of error in the wave models, especially in a small and enclosed basin such as the Mediterranean Sea, where even a limited change in the general atmospheric situation can trigger significant modifications in the local wind patterns (e.g. Bertotti and Cavaleri, 2009a, 2009b). This finding was observed and confirmed in this
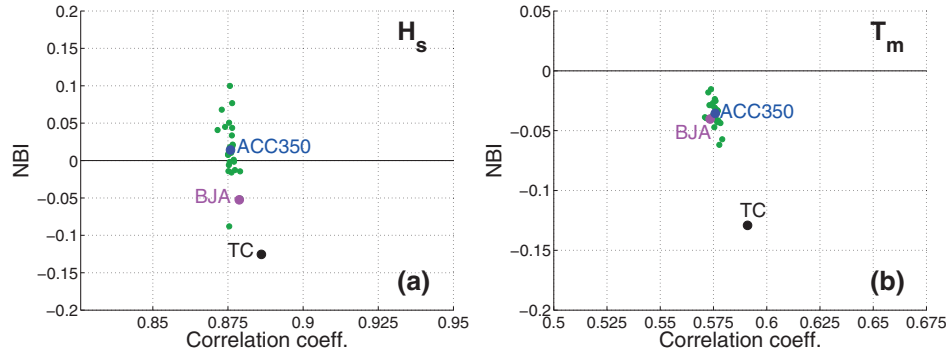
Fig. 3. NBI versus correlation coefficient for the case studies analyzed in the V-10-10 dataset. Each point represents a different parameterization. The results are relative to the significant wave height and average period and are illustrated in panels (a) and (b), respectively.
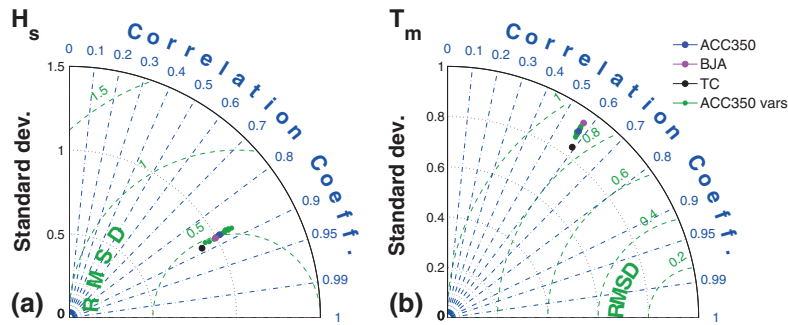

Fig. 4. Taylor diagram for the case studies analyzed in the V-10-10 dataset. Each point represents a different parameterization. The results are relative to the significant wave height and average period and are illustrated in panels (a) and (b), respectively.

Table 4
Statistical indicators *NBI* and *HH* for the significant wave height H_s evaluated for the whole dataset (buoys) in storm and non-storm conditions.

Parameter	Storm conditions (H_s)				Non storm conditions (H_s)			
	NBI		*HH*		*NBI*		*HH*	
	V-10-10	V-20-10	V-10-10	V-20-10	V-10-10	V-20-10	V-10-10	V-20-10
ACC350	−0.1%	−1.4%	0.250	0.265	4.8%	1.7%	0.389	0.404
BAJ	−6.0%	−7.2%	0.256	0.278	−3.3%	−6.1%	0.390	0.409
TC	−12.2%	−13.0%	0.275	0.294	−12.7%	−14.3%	0.386	0.407
DICCA	−1.3%	−3.1%	0.249	0.265	3.4%	0.00%	0.386	0.401

Table 5
Statistical indicators *NBI* and *HH* for the mean wave period $T_{m0,-1}$ evaluated for the whole dataset (buoys) in storm and non-storm conditions.

Parameter	Storm conditions (T_m)				Non storm conditions (T_m)			
	NBI		*HH*		*NBI*		*HH*	
	V-10-10	V-20-10	V-10-10	V-20-10	V-10-10	V-20-10	V-10-10	V-20-10
ACC350	1.6%	1.0%	0.247	0.250	−8.5%	−9.1%	0.303	0.311
BAJ	2.0%	1.5%	0.250	0.253	−9.8%	−10.2%	0.312	0.319
TC	−7.8%	−8.3%	0.259	0.262	−18.0%	−18.3%	0.353	0.358
DICCA	1.3%	0.4%	0.248	0.249	−8.9%	−9.6%	0.306	0.312

analysis by taking into account the different resolutions of wind forcing over the whole computational domain. The use of the lower resolution wind data for the V-20-10 dataset resulted in a slight shift in the bias towards lower values and a small increase in the scatter error for both the significant wave height and the mean period, with respect to the same indicators obtained from the dataset V-10-10, as reported in Table 3. In Tables 4 and 5, we reported the error indicators that were estimated under storm and non-storm conditions (the definition used for storm conditions was given in Section 4.2). This was performed to verify the performance of the model during severe and

moderate sea states. The records used for these analyses were 30,074 for storm conditions and 12,026 for non-storm conditions, and they represent subsets of the V-10-10 and V-20-10 datasets. In the tables, only the results of the most relevant parameterizations are displayed.

The smoothing effect of using lower resolution wind data is more evident under storm conditions, when the value of *HH* found for the V-20-10 dataset was 6.4% higher than the *HH* estimated for V-10-10. In non-storm conditions, the increase in *HH* is instead 3.9%. In Fig. 6(a) and (b), it is also possible to notice how the evolution of the storm is smoothed for dataset V-20-10 compared to V-10-10, especially
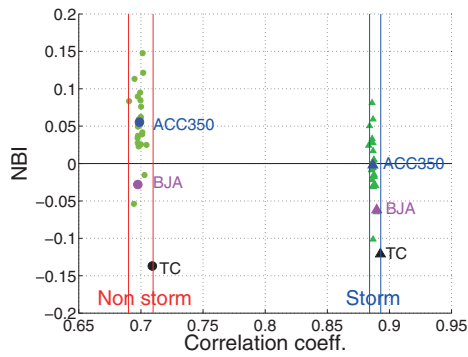
Fig. 5. NBI versus the correlation coeff. of a significant wave height for the case studies analyzed in the V-10-10 dataset. Storm and non-storm conditions.

corresponding to the significant wave height peak. A worsening in the performances may be due to a poorer representation of the mesoscale phenomena by the atmospheric model.

For both the significant wave height and mean period, the bias and mean square error present better values under storm conditions than in non-storm conditions. This is due to the fact that large storms are often triggered by synoptic scale patterns that are well-resolved at larger scales, whereas mesoscale phenomena, which are more difficult to model, can also have a significant impact under non-storm conditions.

6. The role of resolution in modeling mesoscale events

Therefore, a higher resolution in wind forcing is expected to improve the modeling of smaller scale features, in particular, of intense

mesoscale storm events, which are frequent and important in the Mediterranean Sea (e.g. Bertotti and Cavaleri, 2009a, 2009b). It is well known that the interaction of the complex topography of Mediterranean regions with larger scale disturbances frequently induces the formation of secondary mesoscale cyclones (e.g. Buzzi et al., 2003; Menendez et al., 2013) associated with peculiar wind features that can significantly affect wave generation. A number of cyclogenetic areas can be identified when the development of subsynoptic lows is triggered by major North Atlantic synoptic systems being affected by local orography and/or low-level baroclinicity (Trigo et al., 2002). One of these areas is the Gulf of Genoa, where cyclogenesis in the lee of the Alps frequently occurs (Buzzi and Tibaldi, 1978) and can affect the wind and wave regimes of the Ligurian and Tyrrhenian seas. In spring and summer, thermally induced lows become progressively more important, despite the existence of other factors, such as the Atlas Mountains contributing to lee cyclogenesis in northern Africa, or to the extension of the Asian monsoon into the eastern part of the Mediterranean. Consequently, the behavior of Mediterranean cyclones can also be modulated by diurnal forcing, and the triggering and mature stages are mostly reached by late afternoon or early night-time, whereas cyclolysis tends to occur in early morning. (Trigo et al., 2002).

On the other hand, it is known that an excessive resolution in the wind data generally leads to a worsening of "single point indicators" such as *NBI* and *HH*, due to an effect called the double penalty (e.g. Ardhuin et al., 2007; Cavaleri, 2009; Bertotti and Cavaleri, 2009a). This effect occurs when a high resolution model forecasts realistic but misplaced (in space and/or time) patterns, or even not corresponding with observed features, involving a "noisy" simulation. The effect is named the double penalty effect because in such cases, the model is doubly penalized: the first time because it fails to predict certain
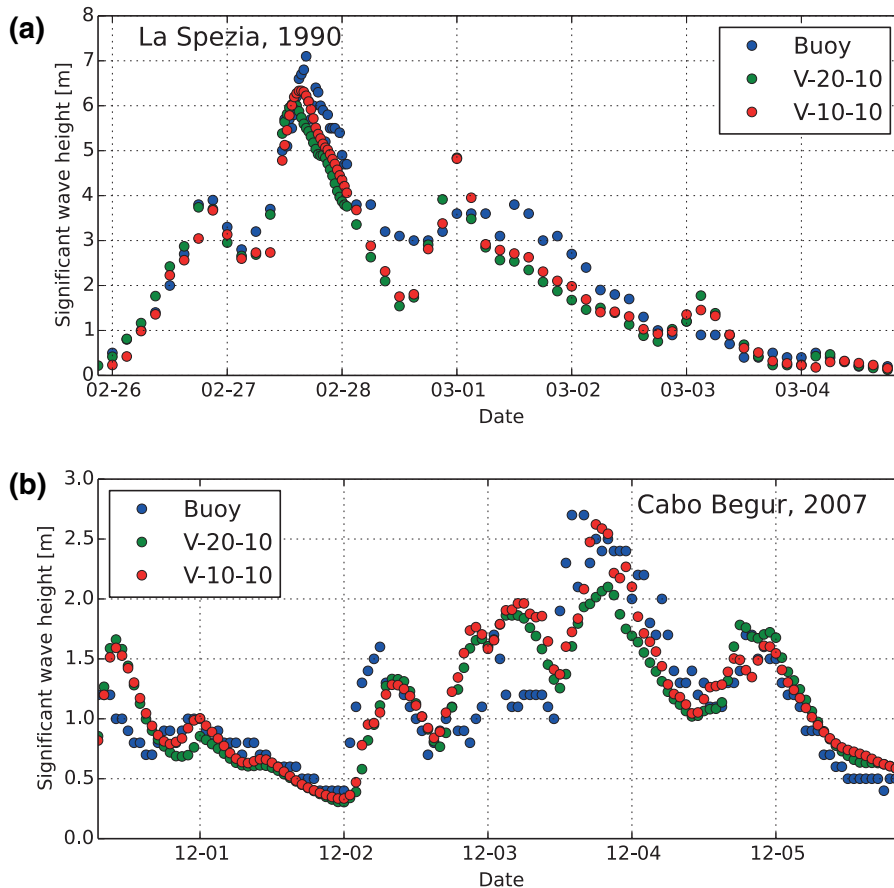

Fig. 6. February 1990 storm, La Spezia (a), and December 2007, Cabo Begur (b). Significant wave height of buoy, V-10-10 and V-20-10 datasets.
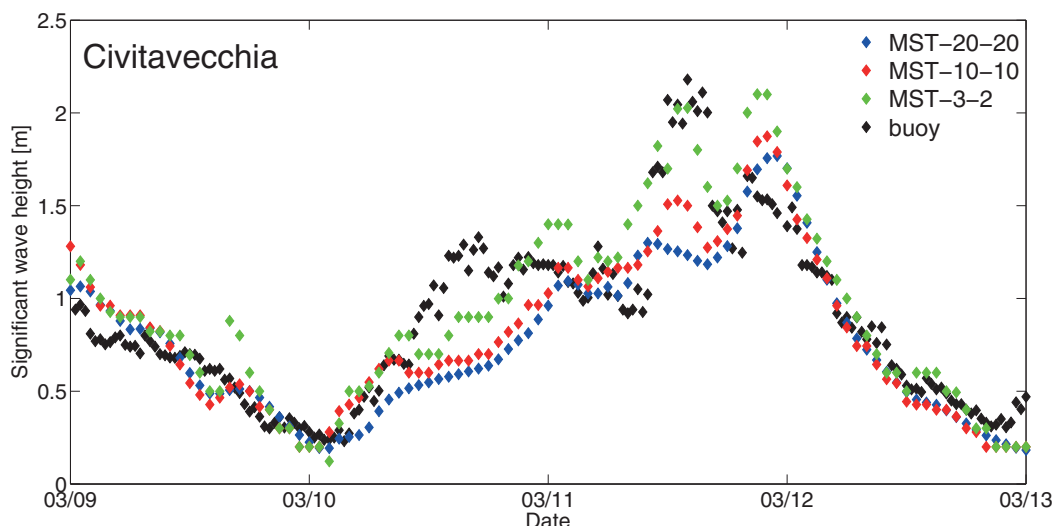
Fig. 7. Mesoscale storm of March 2004 at Civitavecchia, significant wave height of buoys, MST-3-2, MST-10-10 and MST-20-20 datasets. (For interpretation of the references to color in the text, the reader is referred to the web version of this article.)

Table 6
Case studies considered for the analysis of mesoscale events. The maximum wave height refers to records of buoys from Ponza and Civitavecchia.

Case study	Start date	End date	Max H_s [m]	Max T_m [m]
February 2004	20/02/2004	03/03/2004	4.09	7.3
March 2004	08/03/2004	15/03/2004	3.08	7.6
April 2004 (1)	03/04/2004	15/04/2004	3.83	7.7
April 2004 (2)	16/04/2004	23/04/2004	3.81	8.0
August 2004	16/08/2004	25/08/2004	3.17	7.8
February 2005	19/02/2005	25/02/2005	4.35	7.6
April 2005	08/04/2005	15/04/2005	3.28	7.8
December 2005	25/12/2005	01/01/2006	3.91	8.2
August 2006 (1)	09/08/2006	17/08/2006	2.83	7.4
August 2006 (2)	27/08/2006	04/09/2006	3.67	8.4

Table 7
Symmetrically normalized root mean square error *HH* for significant wave height H_s and mean period T_m for the mesoscale events in the Tyrrhenian Sea.

	$HH(H_s)$	$HH(T_m)$
MST-20-20	0.276	0.320
MST-10-10	0.249	0.263
MST-3-2	0.263	0.281

features, and the second time because it predicts some features in the wrong place and at the wrong time. The fact that an increase in the resolution from 20 km to 10 km improves the values of *NBI* and *HH* suggests that in the V-10-10 dataset, the double penalty effect induced by a higher resolution does not yet overcome the benefits of the ability to represent smaller-scale wind patterns.

Therefore, the possibility that a further increase in the resolution may still improve the model performance in a different set of case studies was investigated. Because synoptic scale events can be resolved with sufficient accuracy at coarser resolutions, only mesoscale events (explained in Section 4.1, i.e., associated to relatively small-scale secondary cyclogenesis) were selected for this analysis. To perform this analysis, ten case studies were chosen among storms that occurred in the Tyrrhenian Sea between 2004 and 2006 (see Table 6) and were modeled with different grid settings:

- R20 grid (approximately 20 km of resolution) forced by the 20 km resolution wind data (the dataset obtained with this settings was labeled MST-20-20).
- R10 grid (approximately 10 km of resolution) forced by the 10 km resolution wind data (the dataset obtained with this settings was labeled MST-10-10).
- R2 grid (approximately 2 km of resolution) forced by the 3.3 km resolution wind data (the dataset obtained with this settings was labeled MST-3-2).

In the abbreviations introduced above, MST stands for "Mesoscale on the Tyrrhenian Basin"; the first number is the resolution of the atmospheric model, and the second number is the approximate

resolution of the wave model (both expressed in km). This analysis was carried out using an ACC350 parameterization. The results were compared to observations provided by the buoys from Civitavecchia and Ponza (3,356 records) using the indicators of symmetrically normalized root mean square error *HH* of significant wave height and mean period. The results are reported in Table 7.

Improved performance from a resolution of 20 km to a resolution of 10 km, already found when comparing the V-20-10 and V-10-10 datasets, was confirmed by this analysis, which exhibited a value of *HH* 10.8% higher in the MST-20-20 analysis with respect to MST-10-10 at a significant wave height, and 21.7% higher for the mean period. Improvement in *HH* between MST-20-20 and MST-10-10 with respect to the one between V-20-10 and V-10-10 is partly due to the fact that the strong mesoscale character of the selected case studies in MST-20-20 enhances the smoothing effect of a lower resolution wind forcing. Furthermore, in MST-20-20, the WWIII grid also has a resolution of approximately 20 km (the resolution of the R20 grid), whereas in V-20-10, the WWIII grid has a resolution of approximately 10 km (the resolution of the R10 grid). Conversely, the MST-3-2 analysis presents lower values of *HH* with respect to the MST-10-10 for both the significant wave height and the mean period, suggesting an increased double penalty effect at a resolution of 3 km in the wind fields.

These results indicate that higher resolution wind fields do not necessarily involve an improvement of "single point error indicators" such as *HH*. However, a slight shift in a sharp atmospheric pattern can result in a severe worsening in such indicators, though it is questionable whether this situation always represents a real worsening of the analysis and its qualitative and quantitative information. Fig. 7 illustrates the significant wave height relative to a March 2004 event at the Civitavecchia buoy, for the MST-3-2, MST-10-10 and MST-20-20

Table 8
Error indicators for significant wave height, mean period and mean direction for the 32 years of hindcast analysis realized with ACC350 and DICCA parameterizations.

	H_s		T_m			θ_m	
	ACC350	DICCA	ACC350	DICCA		ACC350	DICCA
NBI	2.8%	1.1%	5.2%	4.7%	*NBI*	1.0%	1.0%
HH	0.336	0.338	0.183	0.182	*NRMSE*	0.132	0.132

datasets and at the buoy. Even if, in this case, the series relative to the MST-3-2 analysis (the green line) may present a similar value of *HH* as the MST-10-10 one (the red line) because it delays the first peak and overestimates the third one, the MST-3-2 provides a better qualitative description of the event and a better estimation of its mature stage. In situations such as the one illustrated in Fig. 7, the results provided by a very high resolution model may be considered more reliable and useful than those obtained at a lower resolution, even if they exhibit worse indicator values like *NBI* and *HH* due to a shift in time for the modeled patterns.

Therefore, good model performance evaluations may be provided by techniques such as Dynamic Time Warping (e.g. Salvador and Chan, 2004) or, more generally, spatial verification approaches whose objective is to identify localized features of interest in scalar fields and to compare features in two fields to identify which features best correspond to each other. When objects have been identified and categorized, the similarity statistics of the objects in the two datasets are computed. Such techniques are increasingly employed in meteorology, especially for verifying the numerical prediction of highly localized, irregular fields such as precipitation (Davis et al., 2009; Gilleland et al., 2009), and they could also be employed to assess wave model predictions if field measurements (e.g., satellite wave height retrievals or radar maps) are available.

7. 32-year (1979–2010) hindcast

On the basis of the model calibration discussed in Section 4.3, we produced a hindcast analysis covering a period from the 1st of January, 1979 to the 31st of December, 2010. The reanalysis was carried out using grid A10 in the WRF model and grid R10 in the WWIII (see Section 2), while both ACC350 and DICCA parameterizations were employed. The hindcast was validated using the entire set of records from Rete Ondametrica Nazionale (RON), Red Exterior (REDEXT) buoys and a set of buoys from the Greek Poseidon network (see Fig. 2). Records with a significant wave height lower than 0.5 m were excluded because they are intrinsically more affected by noise, and because much of the buoy records have a precision of 0.1 m, causing small measurements to be inherently inaccurate (e.g. Jensen et al., 2013). The overall values of the error indicators for the significant wave height, mean period and mean direction are shown in Table 8. In general, we found strong agreement among the model results with observations. The overall improvement of DICCA over ACC350 is rather small: the global normalized bias in significant wave height found for the DICCA parameterization is closer to zero than that of ACC350, but it is still slightly positive. A further reduction in the value of the parameter β_{max} would lead to a vanishing overall bias, but would result in too strong of an underestimation in storm conditions. In Fig. 8, the normalized bias of the significant wave height was plotted as a function of the measured significant wave height. The value of the bias was rather small within an ample range of wave heights, but it tended to be strongly negative under severe conditions and strongly positive for significant wave heights lower than 1 m. The underestimation in storm conditions might be related to the above mentioned smoothing of the mesoscale features, which are characteristic of the atmospheric dynamics in the Mediterranean Basin.
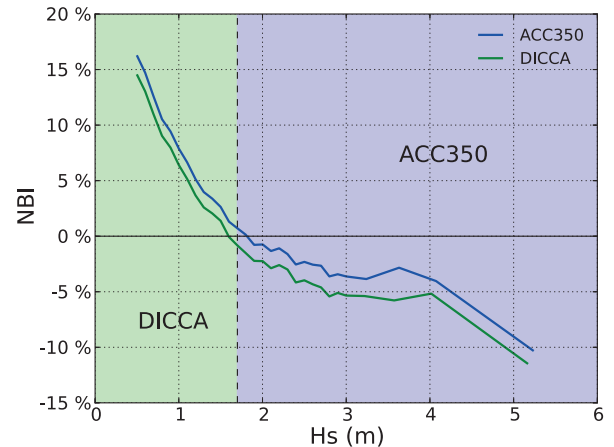
Fig. 8. Normalized bias in significant wave height as a function of the significant wave height, for parameterizations ACC350 and DICCA. In the left area, the DICCA parameterization is less affected by positive bias, whereas in the right area, the ACC350 performs better.

It is worth noting that in Fig. 8, the curve corresponding to the DICCA parameterization is always below the one corresponding to ACC350. This is consistent with the way we estimate the DICCA parameterization, decreasing the wave growth term in order to reduce the overall positive bias of the significant wave height of ACC350. From Fig. 8, a critical value of H_s clearly emerges (approximately 1.7 m) below which the DICCA parameterization works better than the ACC350, and above which the conclusion is opposite. In short, the DICCA parameterization seems to be more suitable for wave forecasting under "normal" conditions. For extreme cases, ACC350 would be preferable.

To provide more localized information about hindcast accuracy, buoys have been grouped on the basis of their location. Different sub-basins are listed in Table 9 together with the corresponding buoys. The error measures are reported in Table 10. Basins characterized by relatively long fetches (Central Mediterranean, Tyrrhenian and Ionian Seas) present significant wave height bias values close to zero, indicating a reliable estimate of the average significant wave height. For basins mainly characterized by short fetches (Adriatic and Aegean seas), the significant wave height bias is negative. This may be related to a tendency in the model to underestimate the wave growth on short fetches. The particularly high value of the mean square error *HH* of the significant wave height estimated for the buoys located in the Greek archipelago is clearly related to the particularly complex orography and bathymetry (resolution does not allow for an accurate representation of bathymetric features, e.g. Tuomi et al., 2013). Finally, the Alboran and Balearic seas show positive values of bias together with low values in the *HH* index of significant wave height. In those basins, the wave climate is characterized in a relevant way by swell coming from East/North-East or West in a direction parallel to the coast (e.g. Cañellas et al., 2007; Sánchez-Arcilla et al., 2008). This finding suggests an underestimation of the sheltering effects of the Balearic archipelago and the Spanish coast at the buoy points. Furthermore, the Spanish Mediterranean coast is a complex area for atmospheric simulation (e.g. Menendez et al., 2013), and related

Table 9
Basins considered for local performances validation.

Basin	Buoys
Adriatic	Ancona, Monopoli, Ortona, Punta Maestra
Alboran	Cabo Gata, Cabo Palos, Alboran
Balearic	Dragonera, Tarragona, Valencia
Aegean	E1M3A, Mykonos, Athos
Ionian	Catania, Crotone, Pylos, Zakynthos
Central Mediterranean	Alghero, Cabo Begur, Mahon, La Spezia
Tyrrhenian	Civitavecchia, Ponza, Cagliari, Capocomino, Cetraro, Mazara, Palermo

Table 10
Error indicators for the significant wave height, mean period and mean direction for buoys grouped by basin.

Basin	H_s		T_m			θ_m	
	ACC350	DICCA	ACC350	DICCA		ACC350	DICCA
Adriatic	Sample size: 83,268						
NBI	−4.5%	−6.15%	0.2%	−0.32%	NBI	2.8%	2.75%
HH	0.323	0.313	0.242	0.242	NRMSE	0.172	0.173
Alboran	Sample size: 93,543						
NBI	12.21%	10.64%	9.08%	8.63%	NBI	−1.1%	−1.09%
HH	0.274	0.266	0.188	0.187	NRMSE	0.105	0.105
Balearic	Sample size: 62,351						
NBI	12.03%	10.16%	7.22%	6.52%	NBI	−0.51%	−0.55%
HH	0.307	0.299	0.17	0.167	NRMSE	0.125	0.125
Aegean	Sample size: 36,319						
NBI	−7.54%	−9.1%	4.15%	3.57%	NBI	3.32%	3.31%
HH	0.507	0.511	0.136	0.134	NRMSE	0.084	0.084
Ionian	Sample size: 72,082						
NBI	1.39%	−0.29%	5.1%	4.72%	NBI	0.89%	0.94%
HH	0.342	0.342	0.197	0.196	NRMSE	0.162	0.162
Central Mediterranean	Sample size: 175,292						
NBI	0.42%	−1.19%	4.87%	4.32%	NBI	1.3%	1.28%
HH	0.359	0.368	0.152	0.149	NRMSE	0.12	0.12
Tyrrhenian	Sample size: 145,357						
NBI	3.49%	2.02%	4.99%	4.59%	NBI	1.22%	1.21%
HH	0.278	0.278	0.195	0.194	NRMSE	0.124	0.124

errors in the wind fields are another possible cause of the relatively high bias in the significant wave height.

7.1. The role of bathymetry resolution

A main issue that emerged during the hindcast validation consists of the generation of systematic errors due to the unresolved features in the bathymetry, which can significantly modify the wave dynamics in proximity to the examined buoys. An example of the relative inaccuracy of the model due to an approximate representation of the bathymetry can be observed for the Catania buoy. The bathymetry at the buoy location is illustrated in Fig. 9: map (c) shows the buoy position with respect to the coastline, map (d) shows, in detail, the bathymetry around the buoy. This buoy is located several kilometers off the eastern coast of Sicily. The buoy is moored at a depth of approximately 40 m. Just eastward from this point, there is a steep continental slope where depths reach up to 1200 m in less than 15 km. Charts (a) and (b) in Fig. 9 show the normalized bias of the significant wave height and the mean direction measured at the buoy for waves coming from each directional octant. The model results at this location are affected by a strong negative bias in the significant wave height, especially for waves coming from the open sea. In particular, waves coming from the E-NE are affected by a strong positive bias in the mean direction, suggesting a general underestimation of the refraction effects. The representation of refraction through an explicit propagation scheme in the $k - \theta$ space can generate problems because the time derivative of θ diverges for vanishing water depths, involving a violation of the CFL condition in the $k - \theta$ space for virtually any time step. However, this is not the case at the Cata-

nia buoy, which is located in a cell where the average water depth is approximately 250 m. Since the time step chosen for spectral propagation is 900 s, the Courant number is below one. Therefore, the relative inaccuracy of the model could be due to the resolution of the model, which is unable to represent the steep profile of the continental slope (the WWIII grid is represented in Fig. 9 by the black dotted lines).

Even if a resolution of approximately 10 km is satisfactory for wind forcing because it provides rather good benchmarks using single point error indicators such as *NBI* and *HH*, it is not enough to adequately represent the bathymetric effects near the coast in many places. On the other hand, a high resolution would not be necessary in the open sea, where no obstacles exist in the path of traveling waves and the bathymetric variations are mild. A way to address this problem is by using the finite elements propagation scheme, which is available in the new version of WWIII (Roland, 2008; Tolman, 2014), which allows for the definition of unstructured grids in the computational domain, thereby refining the resolution where the numerical model needs it.

8. Conclusions

In this study, some characteristic aspects of wave modeling in an enclosed basin like the Mediterranean Sea were examined. A performance assessment of the WRF-WWIII model chain on seventeen storm events led to the conclusion that the source terms of wave growth-dissipation proposed by Ardhuin et al. (2010), set up with a parameterization that incorporates a long swell dissipation term, exhibit the best performance among the available reference settings; this is due to its improved ability for representing and balancing the
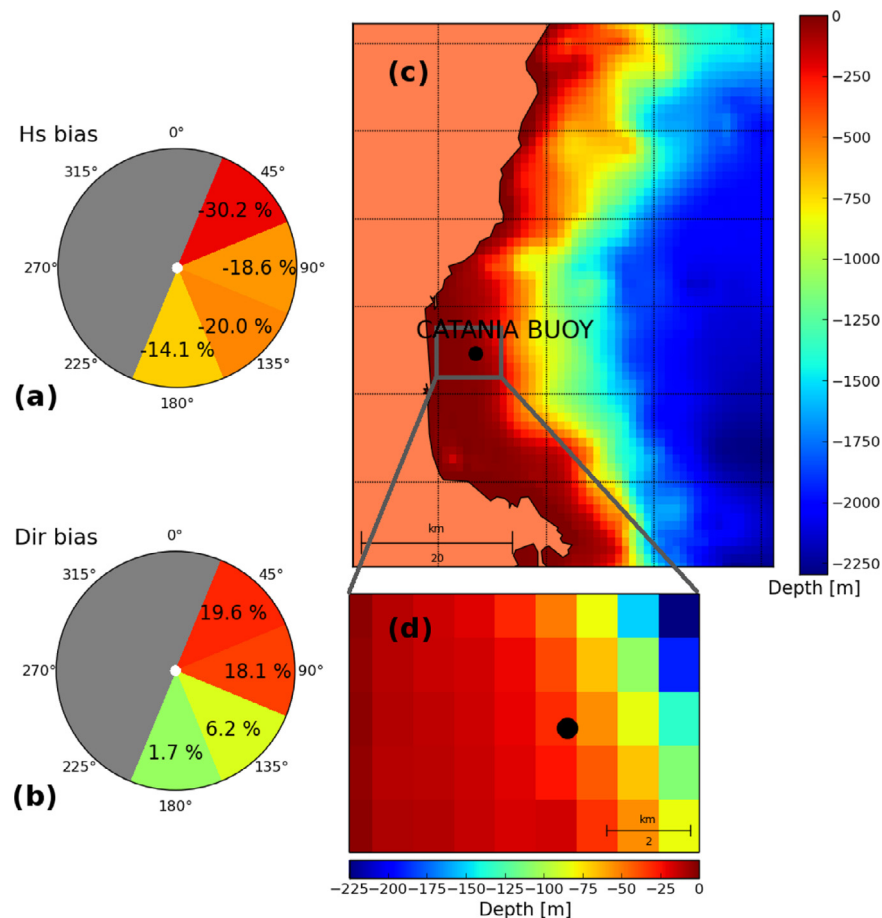
Fig. 9. Bathymetry at the Catania buoy. The black dotted lines represent the WWIII grid. In the charts on the left, the normalized bias of the significant wave height and mean direction at the buoy are shown for waves coming from each directional octant. Octants corresponding to directions from 225° to 360° have not been plotted because the related measures of normalized bias are not significant.

effects of growth and dissipation due to wind forcing, which involves a better representation of the local effects that important for the overall Mediterranean Sea dynamics.

The convenience of downscaling atmospheric input from the original CFSR resolution of about 38 km was verified, forcing a wave model with wind data at different resolutions. This analysis indicated that the wave model forced by 20 km wind data performs appreciably worse than the same model forced by 10 km wind data.

The impact of resolution on the description of mesoscale dynamics was analyzed in a different set of ten case studies characterized by distinct mesoscale features. Increasing the resolution up to set MST-3-2 (resolution of approximately 3 km for wind data and approximately 2 km for the wave model) led to a significant worsening in the values of the symmetrically normalized root mean square error *HH* of significant wave height and mean period, likely as a result of the so-called double penalty effect. However, the ability of single point indicators such as *HH* to assess the performance of the model at these resolutions is questionable because they are scarcely able to quantify the information related to peaks modeled with a shift in space and time. The use of techniques that verify the overall shape of space-time patterns, such as Dynamic Time Warping (e.g. Salvador and Chan, 2004) and the Method for Object-Based Diagnostic Evaluation (MODE; Davis et al., 2009) might provide better indication of the performances of high resolution wave models.

The development of a 32-year wave hindcast analysis was performed to provide an extended database for future applications, such as analysis of the wave climate or studies of the power available for energy harvesting. A validation of the dataset obtained using

reference parameterization of Ardhuin et al. (2010) revealed that the normalized bias of significant wave height is positive for small significant wave heights and decreases for increasingly significant wave heights, turning negative for significant wave heights greater than approximately 1.7 m. For the hindcast analysis, also the set of parameters DICCA, obtained calibrating the value of the parameter β_{max} to reduce a slight positive bias of significant wave height, was employed. This improvement was achieved by inducing a better overall balance between situations characterized by positive bias and situations characterized by negative bias in the significant wave height. An analysis of the model bias of the significant wave height as a function of the measured significant wave height indicates that for calm and moderate seas, the set of parameters DICCA perform better than the reference parameterization, whereas in severe conditions it is more affected by negative bias. The general trend of the model, of overestimating the significant wave height in calm and moderate conditions and underestimating it in severe conditions, suggests the need for a recalibration of the model results based on the modeled local conditions.

Finally, the performance of the model at the Catania buoy, which was characterized by the presence of a complex bathymetry, was analyzed, showing that at this buoy, a resolution of approximately 10 km in a hindcast analysis does not provide a reliable representation of the bathymetric effects, such as refraction and shoaling. This aspect assumes particular relevance in a basin such as the Mediterranean Sea, which is characterized by complex coastal profiles and by relatively short fetches compared to the oceans (Indian, Atlantic and Pacific). A solution for this issue may be the use of unstructured grids, which are available in the new version of WWIII.

Acknowledgments

References

Ardhuin, F., Bertotti, L., Bidlot, J.R., Cavaleri, L., Filipetto, V., Lefevre, J-M., Wittmann, P., 2007. Comparison of wind and wave measurements and models in the Western Mediterranean Sea. Ocean Eng. 34 (34), 526–541.

Ardhuin, F., Chapron, B., Collard, F., 2009. Observation of swell dissipation across oceans RID a-1364-2011. Geophys. Res. Lett. 36, L06607.

Ardhuin, F., Hamon, M., Collard, F., Chapron, B., Queffeulou, P., 2008. Spectral wave evolution and spectral dissipation based on observations: a global validation of new source functions. In: Proceedings, 4th Chinese-German joint symposium on Coastal and Ocean Engineering. Darmstadt, Germany.

Ardhuin, F., Rogers, E., Babanin, A.V., Filipot, J., Magne, R., Roland, A., van der Westhuysen, A., Queffeulou, P., Lefevre, J., Aouf, L., Collard, F., 2010. Semiempirical dissipation source functions for ocean waves. part i: Definition, calibration, and validation. J. Phys. Oceanogr. 40 (9), 1917–1941.

Bertotti, L., Cavaleri, L., 2009a. Large and small wave forecast in the Mediterranean Sea. Nat. Hazards Earth Syst. Sci. 9, 779–788.

Bertotti, L., Cavaleri, L., 2009b. Wind and wave predictions in the Adriatic Sea. J. Mar. Syst. 78 (Supplement), S227–S234.

Bidlot, J., Janssen, P., Abdalla, S., 2007. A revised formulation of ocean wave dissipation and its model impact. Technical Report. ECMWF, Reading, U.K.

Bove, M.C., Brotto, P., Cassola, F., Cuccia, E., Massabò, D., Mazzino, A., Piazzalunga, A., Prati, P., 2014. An integrated PM2.5 source apportionment study: positive matrix factorization vs. the chemical transport model CAMx. Atmos. Environ. 94 (94), 274–286.

Buzzi, A., D'Isidoro, M., Davolio, S., 2003. A case study of an orographic cyclone south of the Alps during the MAP SOP. Quart. J. Roy. Meteor. Soc. 129, 1795–1818.

Buzzi, A., Tibaldi, S., 1978. Cyclogenesis in the lee of Alps: a case study. Q. J. R. Meteorol. Soc. 104 (104), 271–287.

Cañellas, B., Orfila, A., Méndez, F.J., Menéndez, M., Tintoré, J., 2007. Application of a POT model to estimate the extreme significant wave height levels around the balearic sea (western mediterranean). J. Coast. Res. Special Issue N 50, 329–333.

Carvalho, D., Rocha, A., Gómez-Gesteira, M., 2012. Ocean surface wind simulation forced by different reanalyses: comparison with observed data along the Iberian Peninsula coast. Ocean Modell. 56 (56), 31–42.

Cassola, F., Ferrari, F., Mazzino, A., 2015. Numerical simulations of Mediterranean heavy precipitation events with the WRF model: analysis of the sensitivity to resolution and microphysics parameterization schemes. Atmos. Res. submitted for publication

Cavaleri, L., 2009. Wave modeling – missing the peaks. J. Phys. Oceanogr. 39 (11), 2757–2778.

Chawla, A., Spindler, D.M., Tolman, H.L., 2013. Validation of a thirty year wavebrk hindcast using the climate forecast system reanalysis winds. Ocean Modell. 70, 189–206.

Chen, F., Dudhia, J., 2001. Coupling an advanced land-surface/hydrology model with the Penn State/NCAR MM5 modeling system. Part I: model description and implementation. Monthly Weather Rev. 129 (129), 569–585.

Chen, G., Chapron, B., Ezraty, R., Vandemark, D., 2002. A global view of swell and wind sea climate in the ocean by satellite altimeter and scatterometer. J. Atmos. Oceanic Technol. 19 (19), 1849–1859.

Chou, M.D., Suarez, M.J., 1994. An efficient thermal infrared radiation parameterization for use in general circulation models. Tech. Memo. 104606, 3. NASA.

Cox, A.T., Cardone, V.J., Swail, V.R., 2011. On the use of climate forecast system reanalysis wind forcing in ocean response modeling. In: Proceedings, 12th Int. Workshop Wave, Hindcasting, Forecasting, Hawaii, USA.

Davis, C.A., Brown, R., Bullock, R., Halley-Gotway, J., 2009. The method for object-based diagnostic evaluation (MODE) applied to numerical forecasts from the 2005 NSSL/SPC spring program. Weather Forecast. 24 (24), 1401–1415.

Gilleland, E.D., Ahijevych, D., Brown, B.G., Casati, B., Ebert, E.E., 2009. Intercomparison of spatial forecast verification methods. Weather Forecast. 24 (24), 1416–1430.

Hanna, S.R., Heinold, D.W., 1985. Development and application of a simple method for evaluating air quality. Technical Report. American Petroleum Institute, Health and Environmental Affairs Dept, Washington, U.S.A.

Hasselmann, K., 1974. On the spectral dissipation of ocean waves due to white capping. Boundary-Layer Meteorol. 6 (1–2), 107–127. doi:10.1007/BF00232479.

Hasselmann, S., Hasselmann, K., 1985. Computations and parametrizations of the non-linear energy transfer in a gravity-wave spectrum. i: a new method for efficient computations of the exact nonlinear transfer integral. J. Phys. Oceanogr. 15 (11), 1369–1377.

Janjic, Z.I., 2002. Non Singular Implementation of the Mellore-Yamada Level 2.5 Scheme in the NCEP Meso model. NCEP Office Note, No. 437. NCEP.

Janssen, P.A.E.M., 1982. Quasilinear approximation for the spectrum of wind-generated water waves. J. Fluid Mech. 117 (117), 493–506.

Jensen, R.E., Swail, V., Hesser, T.J., Lee, B., 2013. Are wave measures actually ground true? In: 13th International Workshop on Wave Hindcasting and Forecasting and 4th Coastal Hazard Symposium.

Kain, J.S., 2004. The Kaine-Fritsch convective parameterization: an update. J. Appl. Meteorol. Climatol. 43 (43), 170–181.

Komen, G., Hasselmann, S., Hasselmann, K., 1984. On the existence of a fully developed wind-sea spectrum. J. Phys. Oceanogr. 14 (14), 1271–1285.

Komen, G.J., Cavaleri, L., Donelan, M., Hasselmann, K., Hasselmann, S., Janssen, P.A.E.M., 1994. Dynamics and Modelling of Ocean Waves. Cambridge University Press, Cambridge, UK.

Menendez, M., García-Déz, M., Fita, L., Fernández, J., Méndez, F.J., Gutiérrez, J.M., 2013. High-resolution sea wind hindcasts over the Mediterranean area. Clim. Dyn. 42, 1857–1872.

Mentaschi, L., Besio, G., Cassola, F., Mazzino, A., 2013a. Implementation and validation of a wave hindcast/forecast model for the west mediterrenean. J. Coast. Res. Special Issue N 65, 1551–1556.

Mentaschi, L., Besio, G., Cassola, F., Mazzino, A., 2013b. Problems in RMSE-based wave model validations. Ocean Modell. 72, 53–58.

Miles, J.W., 1957. On the generation of surface waves by shear flows. J. Fluid Mech. 3 (02), 185–204.

Mlawer, E.J., Taubman, S.J., Brown, P.D., Iacono, M.J., Clough, S.A., 1997. Radiative transfer for inhomogeneous atmospheres: RRTM, a validated correlated-k model for the long wave. J. Geophys. Res. 102 (102), 16663–16682.

Phillips, O.M., 1985. Spectral and statistical properties of the equilibrium range in wind-generated gravity waves. J. Fluid Mech. 156, 505–531.

Pierson, W.J., Moskowitz, L., 1964. A proposed spectral form for fully developed wind seas based on the similarity theory of s. a. kitaigorodskii. J. Geophys. Res. 69 (24), 5181–5190. http://www.agu.org/pubs/crossref/1964/JZ069i024p05181.shtml.

Roland, A., 2008. Development of WWM II: Spectral wave modelling on unstructured meshes. Ph.D. thesis. Technische Universitat Darmstadt, Institute of Hydraulic and Water Resources Engineering.

Saha, S., Moorthi, S., Pan, H.-L., Wu, X., Wang, J., Nadiga, S., Tripp, P., Kistler, R., Woollen, J., Behringer, D., Liu, H., Stokes, D., Grumbine, R., Gayno, G., Wang, J., Hou, Y.-T., Chuang, H.-Y., Juang, H.-M. H., Sela, J., Iredell, M., Treadon, R., Kleist, D., Van Delst, P., Keyser, D., Derber, J., Ek, M., Meng, J., Wei, H., Yang, R., Lord, S., Van Den Dool, H., Kumar, A., Wang, W., Long, C., Chelliah, M., Xue, Y., Huang, B., Schemm, J.-K., Ebisuzaki, W., Lin, R., Xie, P., Chen, M., Zhou, S., Higgins, W., Zou, C.-Z., Liu, Q., Chen, Y., Han, Y., Cucurull, L., Reynolds, R.W., Rutledge, G., Goldberg, M., 2010. The NCEP climate forecast system reanalysis. Bull. Am. Meteorol. Soc. 91 (8), 1015–1057.

Salvador, S., Chan, P., 2004. FastDTW: toward accurate dynamic time warping in linear time and space. In: KDD Workshop on Mining Temporal and Sequential Data, pp. 70–80.

Sánchez-Arcilla, A., González-Marco, D., Bolaños, R., 2008. A review of wave climate and prediction along the Spanish Mediterranean coast. Nat. Hazards Earth Syst. Sci. 8, 1217–1228.

Semedo, A., Sušelj, K., Rutgersson, A., Sterl, A., 2011. A global view on the wind sea and swell climate and variability from era-40. J. Clim. 5 (24), 1461–1479.

Skamarock, W.C., Klemp, J.B., Dudhia, J., Gill, D.O., Barker, D.M., Wang, W., Powers, J.G., 2008. A Description of the Advanced Research WRF Version 3. Technical Note TN-468+STR. 113 pp. NCAR.

Splinder, D., Chawla, A., Tolman, H.L., 2011. An initial look at the CFSR Reanalysis winds for wave modeling. Technical Note, MMAB Contribution No. 290. NCEP.

Taylor, K.E., 2001. Summarizing multiple aspects of model performance in a single diagram. J. Geophys. Res. 106 (106), 1984–2012.

Thompson, G., Field, P.R., Rasmussen, R.M., Hall, W.D., 2008. Explicit forecasts of winter precipitation using an improved bulk microphysics scheme. Part II: implementation of a new snow parameterization. Monthly Weather Rev. 136 (136), 5095–5115.

Tolman, H.L., 2009. User manual and system documentation of WAVEWATCH III version 3.14. Technical Report. NOAA/NWS/NCEP/MMAB.

Tolman, H.L., 2014. User manual and system documentation of WAVEWATCH III version 4.18. Technical Report. NOAA/NWS/NCEP/MMAB.

Tolman, H.L., Banner, M.L., Kaihatu, J.M., 2013. The NOPP operational wave model improvement project. Ocean Modell. 70, 2–10.

Tolman, H.L., Chalikov, D., 1996. Source terms in a third-generation wind wave model. J. Phys. Oceanogr. 26 (11), 2497–2518.

Trigo, I.F., Grant, R.B., Trevor, D.D., 2002. Climatology of cyclogenesis mechanisms in the Mediterranean. Monthly Weather Rev. 130 (130), 549–569.

Tuomi, L., Pettersson, H., Fortelius, C., Tikka, K., Björkqvist, J.-V., Kahma, K., 2013. Wave modelling in archipelagos. Coast. Eng. 83, 205–220.